Rigid Cluster Decomposition Reveals Criticality in Frictional Jamming

Silke Henkes,[1,*] David A. Quint,[2] Yaouen Fily,[3] and J. M. Schwarz[4,†]
[1]Institute of Complex Systems and Mathematical Biology, Department of Physics, University of Aberdeen, Aberdeen AB24 3UD, Scotland, United Kingdom
[2]Department of Bioengineering, Stanford University and Department of Plant Biology, Carnegie Institute of Washington, Stanford, California 94305, USA
[3]Martin Fisher School of Physics, Brandeis University, Waltham, Massachusetts 02453, USA
[4]Department of Physics, Syracuse Biomaterials Institute, Syracuse University, Syracuse, New York 13244, USA
(Received 1 August 2015; published 15 January 2016)

We study the nature of the frictional jamming transition within the framework of rigidity percolation theory. Slowly sheared frictional packings are decomposed into rigid clusters and floppy regions with a generalization of the pebble game including frictional contacts. Our method suggests a second-order transition controlled by the emergence of a system-spanning rigid cluster accompanied by a critical cluster size distribution. Rigid clusters also correlate with common measures of rigidity. We contrast this result with frictionless jamming, where the rigid cluster size distribution is noncritical.

DOI: 10.1103/PhysRevLett.116.028301

The interplay of constraints, forces, and driving gives rise to the jamming transition in granular media. It is now well established that the frictionless jamming transition has characteristics of both second- and first-order transitions. Both the average coordination number and the largest rigid cluster size jump at the transition, yet there exists a diverging length scale [1–4]. Frictional jamming is more puzzling: The hysteresis observed in the stress-strain rate curves of stress-controlled flow simulations [5–9] and experiments [10] has led to an interpretation as a first-order transition. Yet, signs of second-order criticality appear when treating the fraction of contacts at the Coulomb threshold as an additional parameter [11–13]. To elucidate the frictional jamming transition from a microscopic viewpoint, we extend concepts and tools from rigidity percolation, i.e., the onset of mechanical rigidity in disordered spring networks [14–17], to frictional packings. The former is driven by the emergence of a system-spanning rigid cluster that can be mapped out (in 2D) using the pebble game [18], an improved constraint counting method that goes beyond mean field by identifying redundant constraints. We, for the first time, implement a generalized pebble game for 2D frictional systems and use it to identify rigid clusters in quasistatically [5] sheared packings. As we show below, this allows us to identify a second-order transition where rigid clusters emerge out of a viscous backdrop, connecting stresses and nonaffine motions to the microscopic structure.

Generalized isostaticity.—To establish context, we first review the application of Maxwell constraint counting to jamming [19]. For N particles in d dimensions and a mean number of contacts per particle z, interparticle forces yield $dzN/2$ constraints. Since each particle has $\frac{1}{2}d(d+1)$ translational and rotational degrees of freedom, there are $\frac{1}{2}(N-1)d(d+1)$ total degrees of freedom (subtracting out global degrees of freedom). When these match the force constraints, we arrive at the isostatic criterion, or $dzN/2 = \frac{1}{2}(N-1)d(d+1)$. In the limit $N \to \infty$, $z_{\mathrm{iso}} = d+1$ for frictional granular materials. For frictionless packings, we ignore rotations and obtain the familiar $z_{\mathrm{iso}} = 2d$.

Despite being mean field, i.e., neglecting spatial correlations, isostaticity works seemingly well to locate the jamming transition in static frictionless systems [1]. For frictional systems, however, numerical and experimental evidence point to a range $d+1 < z < 2d$ at the transition, with a matching density range from random loose packing [20] to random close packing. To resolve this conundrum, a *generalized isostaticity* criterion was introduced [11,12], that accounts for contacts at the Coulomb friction threshold providing one less constraint

$$z_{\mathrm{iso}}^{m} = (d+1) + 2n_m/d, \tag{1}$$

where n_m is the mean number of such fully mobilized contacts per particle. Equation (1) describes a *line* of transition points interpolating from $z = d+1$ at $n_m = 0$, corresponding to the friction coefficient $\mu = \infty$ limit, to $n_m = 1$ at $z_{\mathrm{iso}} = 4$, corresponding to the $\mu = 0$ limit [11].

Simulation.—To obtain packings near jamming for the nonconservative frictional interaction, energy minimization is not an option. Instead, we implement a common protocol, simple shear at strain rate $\dot{\gamma}$ in Lees-Edwards boundary conditions. As we decrease the strain rate, we move towards a limit where a set of force-balanced quasistatic states compete with driving and dissipation. The mechanical properties of these states become increasingly relevant as dissipation decreases, as measured by low values of the inertial number $I = \dot{\gamma}\sqrt{m/p}$ [5], where p is the pressure and m is the mass. We use the tools of rigidity percolation to explore them.

We simulate systems of $N = 64$–4096 polydisperse disks in two dimensions interacting according to the Cundall-Strack law [21]. To harmonic purely repulsive normal forces $f_n = k_n\delta$, (δ is the particle overlap), it adds an incremental tangential force $df_{\text{tan}} = k_t dt$, where dt is the tangential sliding since establishing the contact. The friction force is constrained by the Coulomb criterion $|f_t| \leq \mu f_n$; once the threshold is reached, contacts continue to slide at $|f_t| = \mu f_n$ until the direction reverses. The energy injected into the system by shearing is dissipated through linear viscous damping forces, $\mathbf{f}_{ij}^{\zeta} = -\zeta(\mathbf{v}_i - \mathbf{v}_j)$ (cut off such that interparticle forces remain strictly compressive), and a small amount of rotational individual damping. We work in scaled units with mean particle radius $\langle r \rangle = 1$ and unit stiffness $k_n = k_t = 1$. Most results below are in the low-friction $\mu = 0.1$, low-damping $\zeta = 0.1$ limit, for $N = 1024$ particles except where specified otherwise. We report additional results for high $\mu = 1$ and high $\zeta = 1$ in Figs. S4 and S6 in the Supplemental Material [22], respectively. Systems are strained for $T = 10^6$ time units in all cases, corresponding to a strain of 10 system lengths for $\dot{\gamma} = 10^{-5}$ strain rate, and 1 system length for $\dot{\gamma} = 10^{-6}$.

Rigidity percolation.—We decompose packings into rigid clusters using a $(k = 3, l = 3)$ pebble game [18]: First, we associate a pebble with each of the $k = 3$ degrees of freedom of a particle. We then build a constraint network from the contact network where a contact imposing n constraints translates to n bonds; i.e., fully mobilized contacts with $|f_t| = \mu f_n$ yield one bond while contacts with $|f_t| < \mu f_n$ yield two (Fig. S1, [22]). The game recursively moves these pebbles along bonds in the constraint network to assign pebbles to bonds, each pebble-covered bond corresponds to a degree of freedom being independently constrained. We continue until $l = 3$ or more pebbles cannot be assigned. Finally, we map out the rigid clusters for each contact network. This algorithm is an extension of the (2,3) pebble game used in the frictionless case. Please see the Supplemental Material [22] and Fig. S2 for more details.

In Fig. 1, we show the four stages of moving from the simulated packing to the rigid cluster decomposition. The force chains in Fig. 1(a) correspond to the constraint network in Figs. 1(b) and 1(c), with frictional contacts (double bonds) in black, and sliding contacts (single bonds) in red. This network forms the basis for the (3,3) pebble game in Fig. 1(c). In our example, it is possible to assign pebbles to most of the bonds in the network without overconstraining it. In agreement with the beyond-mean field nature of Laman's theorem (see Supplemental Material [22]), a number of leftover pebbles also remain, especially at rattlers but also at connected particles (colored circles). Finally, in Fig. 1(d), we decompose the system into rigid clusters, that is connected regions where no more than the 3 pebbles linked to the global translations and rotations can be found. We find three rigid clusters including a large, system-spanning one. The remaining bonds are floppy, i.e., not rigid with respect to any of their neighbouring bonds. Our example system is globally rigid, in spite of an average z below generalized isostaticity. We show that such configurations are generic below. Let us point out

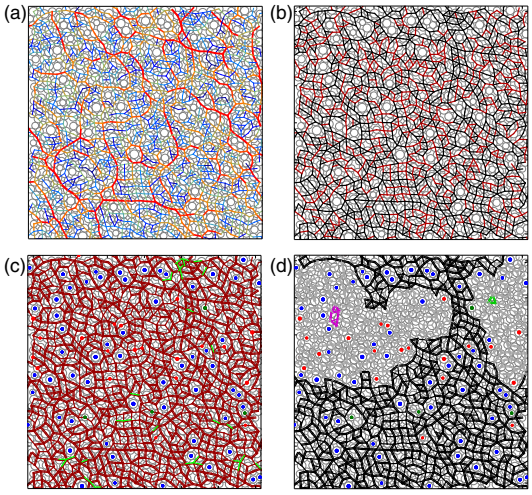

FIG. 1. The pebble game and rigidity percolation for a $N = 1024$ frictional packing. (a) Force chains, with anisotropy due to simple shear. (b) Contact network, with frictional (black) and sliding contacts (red). (c) Result of the (3,3) pebble game where frictional and sliding contacts are mapped to double (thick) and single (thin) bonds, respectively. Red are pebble-covered bonds, green are overconstrained bonds; colored disks are leftover pebbles. (d) Rigid cluster decomposition revealing a partially rigid packing with three rigid clusters (black, purple, and green) and regions of floppy bonds (gray).

that in granular packings, contacts also need to be able to support a compressive load at the given friction coefficient. Therefore, the (3,3) pebble game provides a necessary, but not sufficient condition for rigidity. We discuss the stabilizing role of viscous forces further below.

Results.—We first address how the global properties of the system, including mean stresses and distance from isostaticity, depend on density, strain rate, and system size (Fig. 2). Experimental [10] and simulated frictional systems [6–9] report a hysteresis loop in the stress-strain relations, through a protocol that includes either strain rate ramps or constant stress driving. As a function of density, $\phi = 0.8225$–0.84, we see a transition through jamming, as evidenced by the pressure distribution shifting from a peak at 10^{-4} (in units of overlap) to a peak at 10^{-2} [Fig. 2(a); in Fig. S3 we show that p and σ_{xy} are equivalent]. Since we perform a constant strain rate simulation, we do not observe hysteresis. We instead find intermittent flips between jammed and unjammed states in the transition region, in particular $\phi = 0.8275$ and $\phi = 0.83$ (see Fig. 3). When lowering strain rates, a gap in pressure opens between low and high densities, consistent with an approximately Bagnold scaling $p \sim \dot{\gamma}^{1/2}$ dominated by viscous damping forces below jamming, and the appearance of a yield stress above jamming [Fig. 2(b)]. As intended, the inertial number I in our simulation is in the quasistatic regime $I < 0.001$ for all but the most unjammed packings [Fig. 2(c), inset].

We focus our attention on the parameter $dz = z - z_{\text{iso}}^m$, i.e., the distance from generalized isostaticity. For each $\dot{\gamma}$, all of the data for different packing fractions and system

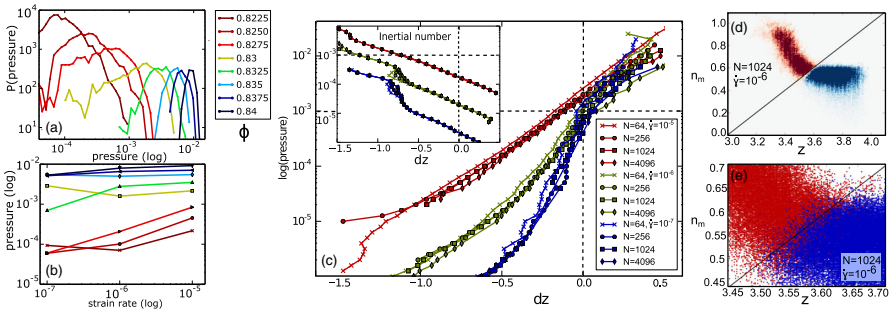

FIG. 2. (a) Pressure distributions for eight densities $\phi = 0.825$–0.84 across the frictional jamming transition, for $N = 1024$ and $\dot{\gamma} = 10^{-5}$. (b) Stress-strain relations for the same ϕ and N, and strain rates $\dot{\gamma} = 10^{-5}$–10^{-7}. (c) Correlation between $dz = z - (3 + n_m)$ and pressure (log scale). Inset: Inertial number I; we are largely in the quasistatic regime $I < 0.001$. (d) Generalized isostaticity: Probability density of the system in (n_m, z_{iso}) phase space, combined from densities $\phi = 0.825$–0.845; $N = 1024$ and $\dot{\gamma} = 10^{-6}$. The red area has $p < 10^{-3}$ and is unjammed, while the blue region has $p > 10^{-3}$ and is jammed. (e) Fluctuations for the same data set, each dot is a jammed (blue) or an unjammed (red) packing.

sizes collapse onto a unique curve $p(dz)$ [Fig. 2(c)]. For the two lower $\dot{\gamma}$, we see two regimes—a rapid drop below $dz \approx 0$ which depends on $\dot{\gamma}$, separated from a more gradual, universal increase at $dz > 0$. The small, positive values of the pressure for $dz < 0$ strongly depend on ζ (see Fig. S5), indicating again that viscous damping forces dominate this regime, consistent with recent results for shear thickening in suspensions [26]. When we visualize our system in a two-dimensional $n_m - z$ phase diagram [Fig. 2(d)], jammed (blue) states defined here by $p \geq 10^{-3}$ exist predominantly in the stable region of the phase diagram below the stability line, while unjammed (red) states mostly exist in the unstable region. There are however significant fluctuations in the transition region with some jammed states below the stability line, suggesting that this mean-field criterion is insufficient [Fig. 2(e)]. System trajectories have roughly equal fluctuations in z and n_m, unlike the avalanching system of Ref. [13], where fluctuations along n_m were more prominent, showing that trajectories depend on driving protocol.

We now present results of the rigid cluster decomposition using the (3,3) pebble game. To demonstrate the

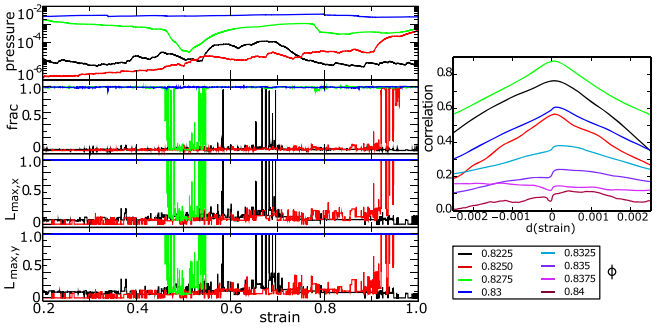

FIG. 3. Temporal correlation between rigidity and stresses. Left: Pressure trajectories for four densities close to jamming (log scale), followed by the fraction (frac) of the system that is rigid, the x length of the largest cluster, and the y length of the largest cluster. Right: Time correlation between pressure and rigidity $\langle \mathrm{frac}(t) \log p(t + dt) \rangle$.

structural importance of the rigid clusters, we first correlate the time series of rigidity and pressure in the region where we observe intermittent behavior (see Fig. 3). In the second, third, and fourth panel, respectively, we show the fraction (frac) of the bonds belonging to a rigid cluster, the x-extent L_x, and the y-extent L_y of the largest cluster (normalized by system size L). Rigid systems are characterized by frac ≈ 1, and system spanning clusters in both directions. All three measures correlate with pressure and with each other, though switches between globally rigid and floppy states are significantly faster than pressure changes. On the right [Fig. 3(b)], the correlation function $\langle \mathrm{frac}(t) \log p(t + dt) \rangle$ shows strong, symmetric correlations for the mostly unjammed runs $\phi = 0.8225$–0.83, and a slight asymmetry indicating that pressure follows rigidity, for the jammed runs $\phi = 0.8325$–0.84.

Figure 2 shows that dz is an appropriate mean-field parameter. From Fig. 3, we conclude that the spatial decomposition indeed plays a role in the macroscopic response of the system. We now ask how rigid cluster analysis can help uncover the nature of the frictional jamming transition. In Fig. 4, top row left, we show the rigid cluster size distribution $p(n)$, where n is the number of bonds per cluster, across the transition. We observe curves characteristic of a *second-order* phase transition, with a $p(n)$ that broadens approaching the transition, and then the emergence of a system-size percolating cluster above the transition. At the transition, we observe a power-law distribution with an exponent $\alpha \simeq -2.5$. For comparison, for connectivity percolation in two dimensions $\alpha = -187/81 = -2.31$ [27] and a self-organized rigidity percolation model yields $\alpha = -1.94$ [28]. To help pinpoint the location of the transition, we plot the maximum cluster length $(L_x^2 + L_y^2)^{1/2}/\sqrt{2}L$ against dz. It approaches unity near $dz = -0.15$ rather than $dz = 0$, consistent with the picture of rigid and floppy regions coexisting in an overall rigid system emerging from Fig. 1. So does an equivalent measure, the spanning probability (Fig. S9). Moreover, this downward shift survives in the large N (Fig. 4 top right) and the $\dot{\gamma} \to 0$ (Fig. S8) limit.

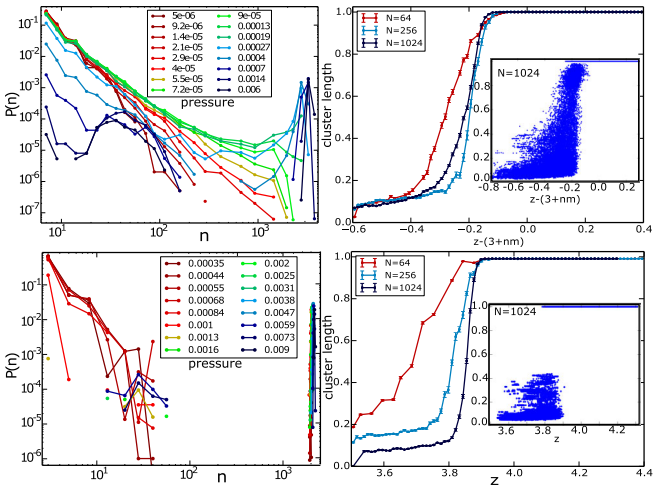

FIG. 4. Rigid cluster size statistics. Left we show the cluster size distribution for pressures across jamming, while on the right is the scaling of the largest cluster size with dz, for three system sizes. Top row: frictional systems, $N = 64$–1024, $\dot{\gamma} = 10^{-6}$, 5 runs each at 8 packing fractions with 160 000 packings in the transition region. Bottom row: frictionless systems, idem with 64000 samples at packing fractions $\phi = 0.835$–0.85.

As comparison, we simulate a frictionless system across its frictionless jamming transition [29] with the same protocol as our frictional runs (Fig. 4, bottom row). Rotations are irrelevant to frictionless disks, so we use a standard (2,3) pebble game here (see Supplemental Material [22]). In stark contrast to the second-order transition above, here we observe the hallmarks of a *first-order* transition: The rigid cluster size distribution is either rapidly decaying at low pressures (most packings have no rigid clusters at all), or markedly bimodal without any intermediate-sized clusters for an order of magnitude. The largest rigid cluster length is gapped (Fig. 4 right, inset), and depends strongly on system size. This finding is consistent with recent results for frictionless systems where packings were found to be either fully rigid or fully floppy [2]. Again, we observe a downward shift in the transition point. Recent work demonstrates that the frictionless transition point can change with protocol [30].

We now address the links between rigid clusters and local forces and displacements (see Fig. 5). First we measure the mean bond normal force scaled by the packing pressure f_n/p for bonds belonging to either a rigid cluster or a floppy region, ensemble averaged over packings with similar dz (left). Below the transition no force difference exists between rigid and floppy regions: viscous forces stabilize isolated rigid clusters and the overall packing is not rigid and has very low pressure. Viscous forces dominate the stresses since no spanning cluster can bear the load. When a percolated rigid cluster structure appears, both its share of the normal force and the pressure rapidly increase with dz; the remaining force on the floppy regions strongly depends on ζ. Finally, the unstable regions become isolated rattlers which bear no load. The gradual decrease

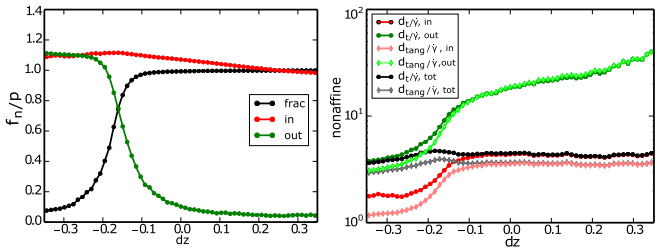

FIG. 5. Correlation between rigid clusters and mechanical stability. Left: Scaled normal force magnitude f_n/p inside (red) and outside (green) the clusters, and the rigid fraction of the system (black). Right: Nonaffine motion (d_t and d_{tang}) inside and outside the clusters, and total.

of nonload bearing rattlers above jamming is well known in static systems [31]; we put it into a dynamical context here for the first time. Spatial correlations in the forces are also found in shear jamming with the transition occurring below the isostatic point [10]. In a pattern resembling swiss cheese, we find that force chain bridge structures bend around convex floppy regions (Fig. S5).

The second measure is the nonaffine motions, which are known to dramatically increase approaching the frictionless [32] and frictional [12] jamming transitions. We measure the relative tangential motion of the centers $\langle |d_t| \rangle$ and tangential sliding at the contacts $\langle |d_{\text{tang}}| \rangle$. Let $\mathbf{r}_{ij} = \mathbf{r}_j(t) - \mathbf{r}_j(t)$ be the vector linking two neighboring particles' centers, $\hat{\mathbf{t}}_{ij}$ the tangential unit vector at the contact, R_i the particle radii, and α_i their angles (see Fig. S1). Then [12,33]

$$d_t^{ij} = \dot{\mathbf{r}}_{ij} \cdot \hat{\mathbf{t}}_{ij}, \qquad d_{\text{tang}}^{ij} = \dot{\mathbf{r}}_{ij} \cdot \hat{\mathbf{t}}_{ij} - (R_i \dot{\alpha}_i + R_j \dot{\alpha}_j). \tag{2}$$

Normalized by the strain rate $\dot{\gamma}$, nonaffine motion is signaled by values above 0.5. For both rigid and floppy regions, above and below the transition, motion is strongly nonaffine (Fig. 5, right, note log scale). However, displacements in floppy regions are much more nonaffine compared to rigid regions, even below the transition where rigid clusters are disconnected, and culminating in values $d_t/\dot{\gamma} > 20$ for isolated rattlers in rigid packings. The normal displacements remain at $d_n/\dot{\gamma} \approx 0.5$ throughout (see Fig. S3). Links between nonaffine buckling and local rigidity have been pointed out previously [34]. We also observe a peak in the total nonaffine motion across the transition.

Conclusions.—In sum, we adapt ideas from rigidity percolation to characterize the frictional jamming transition of slowly sheared packings beyond mean-field. We show that while generalized isostaticity is a good mean-field criterion, spatial correlations do matter: a packing can be jammed below global isostaticity if it contains both floppy regions and a system-spanning rigid cluster, resembling spring networks in this regard. The emergence of such a cluster appears to be first order in frictionless packings, with a sudden jump from microscopic to system-wide clusters, but second order in the frictional case, with a

power law distribution of cluster sizes at the transition. In particular, *partial rigidity* is unique to *frictional* packings. The key instrument in obtaining those new results is rigid cluster decomposition. It allows us to draw connections between disordered spring networks, where partial rigidity is the norm, and granular packings [2,35]. By nature, cluster decomposition ignores contact force constraints. Accordingly, we find that rigidity only correlates with local stresses once arching around floppy regions becomes possible. Conversely, below the transition viscous forces dominate stress, linking our results to granular flow findings [5]. Cluster decomposition, on the other hand, does account for the dynamical nature of fully-mobilized contacts, thus highlighting their central role in frictional packings. Applied strain leads to internal rearrangements, moving through a phase space of rigid, nonrigid, and crucially partially rigid packings due to the second-order nature of the transition. Incorporating this internal variance of accessible states through an internal field, Grob *et al.* were able to explain the phenomenology of hysteresis in frictional jamming [9]. DeGiuli *et al.* [36] also highlight a nonuniversal "sliding-contacts" dominated region of the phase diagram we find ourselves in at $I < 0.001$, $\mu = 0.1$. Our work begins to provide a microscopic basis for such phenomenology.

J. M. S. acknowledges useful discussions with Wouter Ellenbroek and Martin van Hecke and NSF-DMR-1507938 for support. Y. F. acknowledges support from NSF MRSEC, DMR-1420382.

*shenkes@abdn.ac.uk
†jschwarz@physics.syr.edu

[1] C. S. O'Hern, L. E. Silbert, A. J. Liu, and S. R. Nagel, Phys. Rev. E **68**, 011306 (2003).
[2] W. G. Ellenbroek, V. F. Hagh, A. Kumar, M. F. Thorpe, and M. van Hecke, Phys. Rev. Lett. **114**, 135501 (2015).
[3] M. Wyart, S. R. Nagel, and T. A. Witten, Europhys. Lett. **72**, 486 (2005).
[4] C. P. Goodrich, W. Ellenbroek, and A. J. Liu, Soft Matter **9**, 10993 (2013).
[5] F. da Cruz, S. Emam, M. Prochnow, J.-N. Roux, and F. Chevoir, Phys. Rev. E **72**, 021309 (2005).
[6] M. Otsuki and H. Hayakawa, Phys. Rev. E **83**, 051301 (2011).
[7] C. Heussinger, Phys. Rev. E **88**, 050201 (2013).
[8] M. P. Ciamarra, R. Pastore, M. Nicodemi, and A. Coniglio, Phys. Rev. E **84**, 041308 (2011).
[9] M. Grob, C. Heussinger, and A. Zippelius, Phys. Rev. E **89**, 050201 (2014).
[10] D. Bi, J. Zhang, B. Chakraborty, and R. P. Behringer, Nature (London) **480**, 355 (2011).
[11] K. Shundyak, M. van Hecke, and W. van Saarloos, Phys. Rev. E **75**, 010301 (2007).
[12] S. Henkes, M. van Hecke, and W. van Saarloos, Europhys. Lett. **90**, 14003 (2010).
[13] S. Henkes, C. Brito, O. Dauchot, and W. van Saarloos, Soft Matter **6**, 2939 (2010).
[14] P. G. DeGennes, J. Phys. Lett. **37**, L1 (1976).
[15] S. Feng and P. N. Sen, Phys. Rev. Lett. **52**, 216 (1984).
[16] D. J. Jacobs and M. F. Thorpe, Phys. Rev. Lett. **75**, 4051 (1995).
[17] C. Moukarzel and P. M. Duxbury, Phys. Rev. Lett. **75**, 4055 (1995).
[18] D. J. Jacobs and B. Hendrickson, J. Comput. Phys. **137**, 346 (1997).
[19] J. C. Maxwell, Philos. Mag. **27**, 250 (1864).
[20] G. Y. Onoda and E. G. Liniger, Phys. Rev. Lett. **64**, 2727 (1990).
[21] P. Cundall and O. D. L. Strack, Gotechnique **29**, 47 (1979).
[22] See Supplemental Material at http://link.aps.org/supplemental/10.1103/PhysRevLett.116.028301, which includes Refs. [23–25], for details of the modified pebble game algorithm, supplementary simulation results, and a movie of the critical region.
[23] G. Laman, J. Eng. Math. **4**, 331 (1970).
[24] A. Lee and I. Streinu, Discrete Mathematics **308**, 1425 (2008).
[25] T.-S. Tay and J. Comb, Theory Ser. B **36**, 95 (1984).
[26] M. Wyart and M. E. Cates, Phys. Rev. Lett. **112**, 098302 (2014).
[27] A. Aharony and D. Stauffer, 2nd ed., *Introduction to Percolation Theory* (Taylor & Francis, London, 1994).
[28] M. A. Briere, M. V. Chubynsky, and N. Mousseau, Phys. Rev. E **75**, 056108 (2007).
[29] P. Olsson and S. Teitel, Phys. Rev. Lett. **99**, 178001 (2007).
[30] T. Bertrand, R. P. Behringer, B. Chakraborty, C. S. O'Hern, and M. D. Shattuck, arXiv:1506.05041.
[31] S. Atkinson, F. H. Stillinger, and S. Torquato, Phys. Rev. E **88**, 062208 (2013).
[32] W. G. Ellenbroek, E. Somfai, M. van Hecke, and W. van Saarloos, Phys. Rev. Lett. **97**, 258001 (2006).
[33] E. Somfai, M. van Hecke, W. G. Ellenbroek, K. Shundyak, and W. van Saarloos, Phys. Rev. E **75**, 020301 (2007).
[34] A. Tordesillas, Philos. Mag. **87**, 4987 (2007).
[35] J. H. Lopez, L. Cao, and J. M. Schwarz, Phys. Rev. E **88**, 062130 (2013).
[36] E. DeGiuli, J. McElwaine, and M. Wyart, arXiv:1509.03512.